RESEARCH ARTICLE | DECEMBER 30 2025

Temperature-induced absolute energy shift of the electronic spectrum in HgTe nanocrystals

Tommaso Gemo ; Dario Mastrippolito ; Mariarosa Cavallo ; Giorgia Strobbia ; Albin Colle ; Marco Paye ; Jiho Roh ; Adrien Khalili ; Clement Gureghian ; Erwan Bossavit ; Sandrine Ithurria ; Yoann Prado ; Sébastien Sauvage ; Mathieu G. Silly ; Nicolas Péré-Laperne ; Debora Pierucci ; Emmanuel Lhuillier

Appl. Phys. Lett. 127, 263302 (2025)
https://doi.org/10.1063/5.0308025

Applied Physics Letters ARTICLE pubs.aip.org/aip/apl

Temperature-induced absolute energy shift of the electronic spectrum in HgTe nanocrystals

Cite as: Appl. Phys. Lett. **127**, 263302 (2025); doi: 10.1063/5.0308025
Submitted: 20 October 2025 · Accepted: 10 December 2025 ·
Published Online: 30 December 2025

Tommaso Gemo,[1,2] Dario Mastrippolito,[1,3] Mariarosa Cavallo,[1] Giorgia Strobbia,[1] Albin Colle,[1] Marco Paye,[1] Jiho Roh,[1] Adrien Khalili,[1] Clement Gureghian,[1] Erwan Bossavit,[1,3] Sandrine Ithurria,[4] Yoann Prado,[1] Sébastien Sauvage,[5] Mathieu G. Silly,[3] Nicolas Péré-Laperne,[2] Debora Pierucci,[1] and Emmanuel Lhuillier[1,a)]

AFFILIATIONS

[1]Sorbonne Université, CNRS, Institut des NanoSciences de Paris, 4 place Jussieu, 75005 Paris, France
[2]LYNRED, Actipole—CS 10021, 364 route de Valence, 38113 Veurey-Voroize, France
[3]Synchrotron SOLEIL, L'Orme des Merisiers, Départementale 128, 91190 Saint-Aubin, France
[4]Laboratoire de Physique et d'Etude des Matériaux, ESPCI, PSL Research University, Sorbonne Université, CNRS, 10 rue Vauquelin, 75005 Paris, France
[5]Centre de Nanosciences et de Nanotechnologies, CNRS, Université Paris-Saclay, 91120 Palaiseau, France

[a)]**Author to whom correspondence should be addressed:** el@insp.upmc.fr

ABSTRACT

Mercury telluride (HgTe) nanocrystals (NCs) are promising materials for infrared photodetection due to their size-tunable band edges and compatibility with colloidal synthesis. While optical studies have established the temperature dependence of their relative bandgaps, the evolution of their absolute electronic spectrum with cooling remains poorly understood, despite its critical role in the device operation. In this work, we investigate *in situ* the temperature-induced absolute energy shift of HgTe NCs' electronic states with varying band edge energies, using X-ray photoemission spectroscopy. We observe a systematic and reversible rigid shift of core levels toward lower binding energies upon cooling, reaching approximately 80 meV per 100 K, four times larger than the corresponding optical band edge shift (≈20 meV). This behavior is consistent across different NC sizes, making the impact more dramatic for the narrower bandgap NCs. Such absolute energy shifts can significantly alter carrier densities and interfacial band alignments, potentially creating Schottky barriers and reducing extraction efficiency in photodiode architectures. Our findings highlight the necessity of accounting for temperature-induced absolute energy shifts in the design of next-generation HgTe NC-based infrared detectors.

Semiconductors, through their strong interaction with light and their ability to be electrically driven, are central building blocks of optoelectronics. In the visible range, despite its indirect bandgap, which leads to weak absorption and prevents efficient light emission, silicon plays a key role in CMOS sensors and solar cells. The massive integration of Si-based technology has significantly advanced the understanding of this material. Its structural and electronic parameters are known with great accuracy, enabling modeling of the electronic structure across the entire Brillouin zone using 30-band $k\cdot p$ methods.[1–3] When it comes to infrared wavelengths, silicon, with its 1.12 eV bandgap, becomes ineffective, and alternatives must be used.

Among the most mature platforms, HgTe is highly valued because of its ability to cover the entire infrared range, either through alloying[4] or quantum confinement.[5,6] This spectral tunability is enabled by the specific electronic structure of bulk HgTe [see Fig. 1(a)]. Compared to other II–VI semiconductors, the heavier atomic mass increases the spin–orbit (SO) coupling and generates an inverted band ordering. As a result, the Γ_6 symmetry band is not the conduction band (CB) but lies deep in the valence band. In the literature, the negative bandgap of HgTe [ranging from −0.15 eV at room temperature to −0.3 eV at 4 K, see Fig. 1(e)] describes how far the Γ_6 band is located below the Fermi energy. The Γ_8 bands, usually acting as valence bands (heavy hole, HH, and light hole, LH), now lie closest to the Fermi level and become the optically active bands. HgTe is also a semimetal (i.e., a zero-bandgap semiconductor) because the LH and HH bands meet at the Brillouin zone center. Optical transitions in HgTe occur between the HH and LH bands. Under quantum confinement, the transition shifts from the Γ point to a larger wavevector

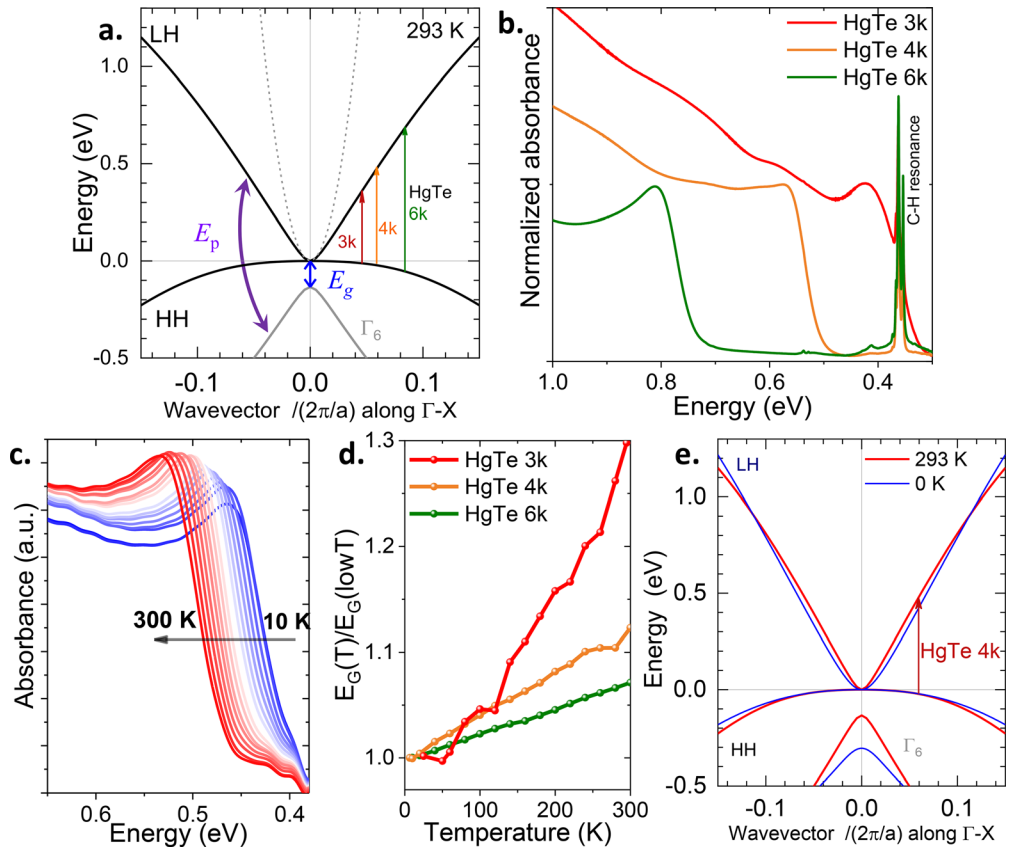

FIG. 1. Electronic structure of HgTe and thermal dependence of the optical spectrum. (a) Electronic structure of bulk HgTe at 300 K for states around the Fermi level using a 14-band k.p formalism. The dotted line is the effective mass parabolic dispersion. (b) Absorption spectra of HgTe NCs with three different sizes associated with HgTe 6k, 4k, and 3k studied throughout the text. The peak at 0.36 eV corresponds to the C–H resonance from ligands. (c) Absorption spectra from HgTe 4k at various temperatures showing a redshift of the band edge as the temperature is reduced. (d) Band edge energy normalized by its low temperature (10 K) value for the three sizes of HgTe NCs under consideration. (e) Electronic structure of bulk HgTe at 293 and 0 K. Data from parts (a), (d), and (e) are adapted, with permission from Moghaddam *et al.*, "The strong confinement regime in HgTe two-dimensional nanoplatelets," J. Phys. Chem. C **124**(42), 23460–23468 (2020). Copyright 2020 American Chemical Society.

given by π/L, with L being the confinement length. The curvature of the HH and LH bands is highly asymmetric (unlike PbS, where they are similar). The HH band has an effective mass close to that of the free electron, while the LH band disperses much more strongly. This results in a conduction band effective mass typically 2 orders of magnitude lighter than that of the valence band.[7] For bulk and thin films, this yields high electron mobility ($>10^4\,cm^2\,V^{-1}\,s^{-1}$ range at room temperature[8,9]). In quantum-confined HgTe, quantization produces a stronger confinement energy for electrons than for holes. Combined with the absence of a bulk bandgap and the large dielectric constant of the material ($\varepsilon_r = 10$–20),[10] which weakens Coulomb corrections, the energy of an optical transition in HgTe quantum dots is dominated by electron confinement energy. As shown in Fig. 1(a), it is worth noting that the LH band dispersion is extremely non-parabolic and only overlaps with a parabolic dispersion (dotted line) over ≈1% of the Brillouin zone, while its dispersion is mostly linear across the most relevant wavevector range.[7] Figure S1 quantitatively illustrates this significant difference, both near the Brillouin zone center and farther away.

Colloidal nanocrystals (NCs) provide a strategy to grow HgTe in the quantum confined regime.[5,6,11] Over the past decade, they have emerged as a promising platform for the development of infrared sensors and imagers. In nanoparticle form, the electronic spectrum results from the interplay of bulk electronic structure, quantum confinement, and surface chemistry, making their spectra more complex. However, advanced integration cannot be achieved without a thorough understanding of the electronic structure. The first step in this direction is the choice of particle size, which determines the band edge energy through quantum confinement. Here, sizes are chosen to be large enough so that their bandgap is clearly below that of silicon and instead matches the range covered by InGaAs technology and mid-IR detectors for the narrowest bandgap. By tuning the HgTe particle size in the 6–12 nm range, the band edge can be adjusted from the short-wave infrared (SWIR, 1.8 μm cutoff) to the extended SWIR (2.5 μm cutoff) and up to the mid-wave infrared (MWIR, 3 μm cutoff) for room temperature absorption, as shown in Fig. 1(b). The HgTe NCs are grown using the procedure given in Ref. 12 and will be later referred to their room temperature band edge given in wavenumber.

For example, HgTe 4k relates to HgTe NCs with a 4000 cm^{-1} (2.5 μm or 0.5 eV) band edge.

For infrared sensors, an important consideration is the operating temperature. As the targeted cutoff wavelength increases, the band edge energy decreases, and thus the photoactivation of carriers that generate photocurrent increasingly competes with phonon activation. As a result, the operating temperature decreases with increasing wavelength. For example, room temperature is still suitable for SWIR sensing, but in the MWIR range, cryogenic conditions (80–200 K, depending on the cutoff and performance targets) remain the norm, though progress toward room temperature operation has been made recently.[13–15] In a photoconductive device, the current density is given by the following equation:[16]

$$J = e.n(T) \cdot \mu(T).F, \tag{1}$$

where e is the elementary charge, $n(T)$ the carrier density, $\mu(T)$ the carrier mobility, and F the applied electric field. The carrier density is the sum of two terms,

$$n(T) = n_{dark}(T) + n_{light}(T), \tag{2}$$

where $n_{dark}(T)$ is the density at equilibrium and is strongly thermally activated. For NCs, the activation energy usually ranges from $E_{BE}/2$[17] to $E_{BE}/10$, where E_{BE} is the optical band edge, which depends on the specific material, surface chemistry, and native doping. This typically corresponds to an activation energy in the 100–200 meV range (Fig. S3). Reducing $n_{dark}(T)$ is the main motivation for cooling. $n_{light}(T)$ is the light-induced carrier density, which depends on the material's absorption cross section and the photocarrier lifetime. This term generally shows a much weaker thermal dependence, driven mainly through the temperature dependence of the carrier lifetime.[14]

In NCs, charge transport occurs via hopping conduction, which introduces a thermally activated behavior of the mobility. The associated activation energy is usually much smaller (in the order of tens of meV) than that of the carrier density. Nevertheless, it also influences the photocurrent. Consequently, an optimal operating temperature exists that minimizes the dark current without significantly degrading the photocurrent. As mentioned above,

$$n_{dark}(T) \propto \exp(-E_{BE}/[\gamma.k_b.T]), \tag{3}$$

with k_b the Boltzmann constant and γ a material-dependent term, but typically in the 2–10 range. In such an expression, the bandgap is assumed to remain constant; however, in practice, it also shifts with temperature, as shown in Fig. 1(c). In bulk HgTe, cooling leads to a redshift.[18,19] This behavior is also observed in the case of NCs[7,20] [Fig. 1(c)], but the shift depends on the particle size and can even flip sign for the most confined form of HgTe.[7] A misleading interpretation will be to assume that lattice contraction upon cooling leads to a change in NC size and therefore to quantum confinement. Such an effect appears negligible.[20,21] The thermal dependence of the optical energy transition actually results from the thermal dependence of the term E_g [the Γ_6–Γ_8 gap; see Fig. 1(e)], which results from electron–phonon coupling. With cooling, E_g increases, affecting the curvature of the LH band through the coupling term E_p[22] (also called the Kane parameter). In other words, as the temperature changes, the effective mass is affected [Fig. 1(e)], and this tunes the electron confinement energy and, therefore, the optical bandgap magnitude. Since optical probing only ascertains the difference in energy between the bands, it remains unclear how a given band shifts in absolute value, which is the focus of this paper. This dependence of the optical bandgap generates a refinement to Eq. (3), since the band edge itself depends on the temperature: $n_{dark}(T) \propto \exp(-E_{BE}(T)/[\gamma.k_b.T])$.

Optical measurements are well-suited to capture changes in the energy difference between bands but miss possible variations in absolute energy. However, absolute band alignment is critical for charge conduction. The best-performing HgTe NC-based detection devices rely on photodiode stacks.[23–28] In such devices, the HgTe NC absorbing layer is surrounded by charge transport layers. Their role is to selectively extract one type of carrier through resonant band alignment with the desired band while maintaining a significant offset with the other band to act as a tunnel barrier, preventing the transfer of carriers through their limited transparency. The design of these diodes depends on accurately determining the energy of each band on an absolute energy scale—either relative to vacuum, as in photoemission measurements, or relative to a reference electrode potential, as in electrochemical studies. Measurements are generally performed at room temperature and are often assumed to remain only marginally affected under operating conditions. However, this assumption must be verified, since potential shifts in absolute energy could introduce Schottky barriers that reduce the photocarrier extraction efficiency or alter carrier density profiles. Addressing this issue requires *in situ* measurements, which cannot be performed with electrochemistry at cryogenic temperatures, as electrolytes freeze and lose their ability to control the Fermi level. For this reason, we focus here on *in situ* X-ray photoemission spectroscopy (XPS) conducted across a temperature range relevant to infrared sensor operation with HgTe NCs.

To initiate this study, we use a series of HgTe NCs, as previously introduced, presenting a band edge in the SWIR, extended SWIR, and MWIR. The electronic spectrum of these NCs is studied using XPS (PHI GENESIS setup, source Al K_α at 1486.6 eV with 100 μm spot size), where a high-energy photon source (i.e., far above the material's work function) is shone on the sample and promotes an electron out of the sample. Its energy is measured with an electron analyzer, allowing the determination of its binding energy (BE) through the energy conservation law. The binding energy provides direct evidence on the semiconductor doping and chemical environment. To conduct such a measurement, the ligand-exchanged NCs are deposited on a gold-coated silicon substrate. This procedure presents a dual benefit: (i) by increasing the film's conductance, we reduce the risk of photo-induced shifts of the photoemission spectrum; moreover, (ii) it matches the procedure used to deposit the active layer in a photodiode, so that the measured NCs experience the same dielectric environment. The survey spectrum acquired at room temperature [Fig. 2(a)] displays contributions from Hg, Te, and C. The latter directly relates to the ligand capping the NCs: mercaptoethanol in this case. It is worth stressing that despite being in prepared in air and the lack of an annealing step, the films do not display any contribution from O 1s, which is expected to have a binding energy (BE) of 532 eV, consistent with the previously reported robustness of the material against oxidation.[29]

We then further track the Hg 4f and Te 4d core levels, acquiring high-resolution spectra. Hg 4f [Fig. 2(b)] comes as a doublet due to the spin–orbit (SO) coupling of the 4f orbital ($4f_{5/2}$ and $4f_{7/2}$, SO splitting = 4.1 eV), with each peak slightly asymmetric toward higher

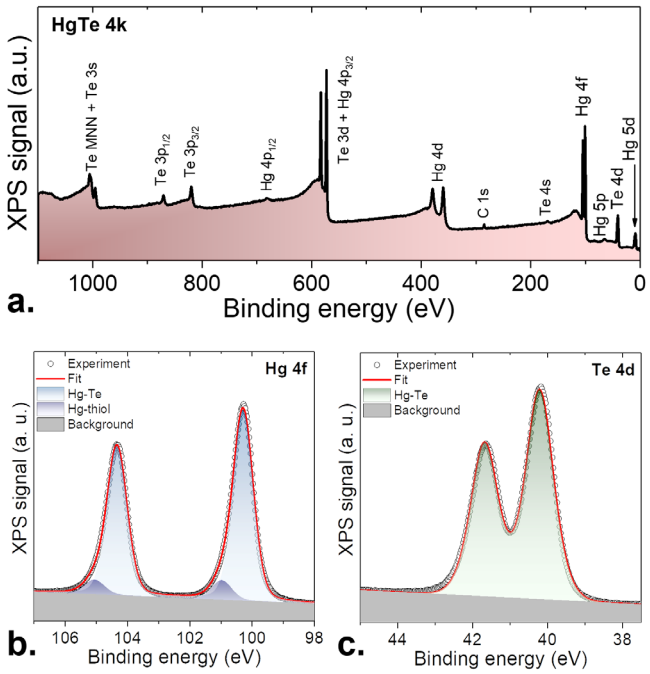

FIG. 2. X-ray photoemission spectra from HgTe NCs. (a) Survey spectra acquired at 1486.6 eV for HgTe 4k NCs. (b) [respectively (c)] Hg 4f (respectively Te 4d) core level from HgTe 4k NCs. Data have been acquired at room temperature.

binding energy. Decomposition of the spectrum reveals a main contribution (Hg $4f_{7/2}$ BE = 100.3 eV) related to Hg bound to Te, while a second weaker contribution (Hg $4f_{7/2}$ BE = 101.0 eV) presents a relative weight that depends on the incident photon energy.[29] The latter is more intense using surface-sensitive conditions (i.e., low photon energy) and was therefore associated with Hg surface atoms bound to thiols (present in the ligands). In the case of the Te 4d state [Fig. 2(c)], a single contribution appearing at BE = 40.2 eV (Te $4d_{5/2}$) is attributed to Te bound to Hg, with a 1.5 eV SO splitting.

We then cool the sample over a temperature range relevant for infrared detection and matching our instrument capability (i.e., down to 173 K in our laboratory setup and down to 80 K, as shown in the supplementary material, at the TEMPO beamline at synchrotron SOLEIL). We observe a shift in the core level toward lower binding energies; see Fig. 3(a). The shift is observed for all sizes of NCs [Fig. 3(b) and S4]. Notably, the shift is fully reversible, and warming the sample restores the spectrum to its initial BE value (Fig. S5).

The shift appears as a rigid shift of the whole photoemission spectrum, since similar shifts are also observed for Te 4d and Te 3d (Fig. S6) core levels and the valence band; see Fig. S7. We confirmed that the observed shift is not related to any artifacts of our setup, as the same behavior was consistently observed in measurements performed on a different setup at a synchrotron facility (Fig. S8). Upon cooling, the drop in the carrier density is expected to make the sample more resistive, which may favor photocharging (i.e., accumulation of photoholes). However, the latter should lead to an increase in binding energy, whereas we observe the opposite trend. Therefore, we can exclude that photocharging is at the origin of the observed behavior.

It is interesting to note that the BE redshift is quite large, reaching around 80 meV already at 173 K, and saturates at about 100 meV at 80 K (see Fig. S8). This shift magnitude must be compared with the tuning of the optical bandgap under the same cooling [Figs. 1(c) and 1(d)], which redshifts by about 20 meV only ($\approx$200 μeV K^{-1},[7] slightly larger for large NCs). This suggests that, on an absolute energy scale, both the valence and conduction bands shift with temperature, and that the difference in their relative shift rates is smaller than their overall energy displacement.

To finish, we propose a reconstructed energy diagram for the three sizes of HgTe NCs under cryogenic conditions [Fig. 4(a)], accounting for both the change in the optical bandgap and the shift of the bands relative to the Fermi level. To determine this graph, the

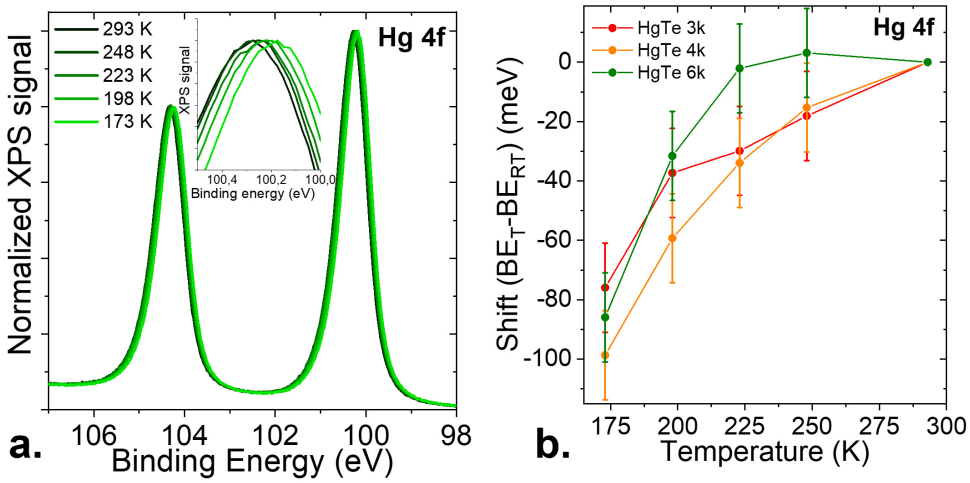

FIG. 3. Temperature-induced shift of the electronic spectra. (a) Hg 4f core level acquired at 1486.6 eV for HgTe 4k NCs under various temperatures. The inset is a zoom on the peak relative to the Hg $4f_{7/2}$ state. (b) Temperature-induced shift of the Hg 4f core level, showing a drop in the binding energy, for three sizes of HgTe NCs. Data relative to Te 3d, Te 4d, and the valence band can be found in Figs. S6 and S7.

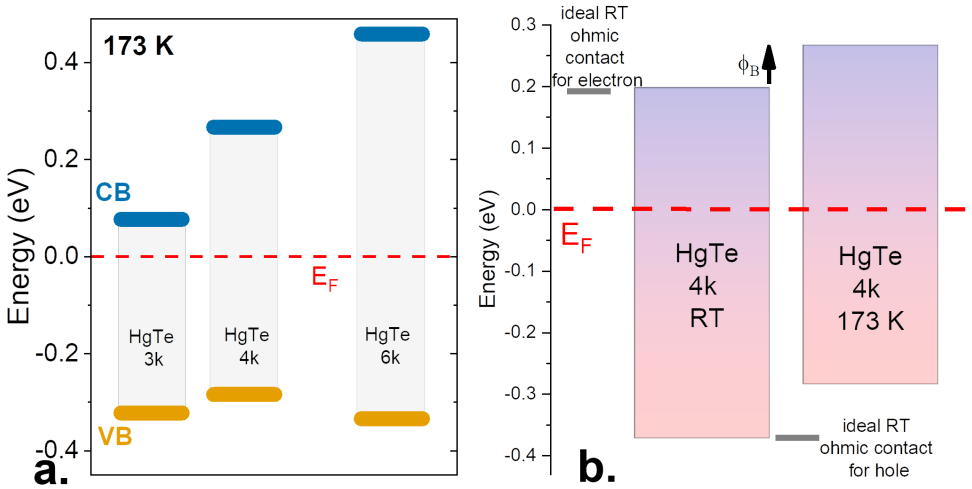

FIG. 4. Effective electronic spectra for HgTe NCs. (a) Valence band (VB), conduction band (CB), and Fermi level (E_F) for three sizes of HgTe NCs, measured at 173 K (i.e., lowest temperature of the XPS setup). (b) Bandgap energy for the HgTe 4k at room temperature and at 173 K, highlighting the formation of a Schottky barrier for the electron.

signal relative to the valence band is measured at room temperature and in cryogenic conditions (Fig. S9) and is used to determine the energy of the valence band maximum with respect to the Fermi level. Then, the energy of the conduction band minimum is determined relative to the valence band by adding the optical bandgap. This relies on the assumption that there is no Coulombic correction for the excitonic structure, an assumption motivated by the large dielectric constant of HgTe.[10] For the low temperature dataset, we account for the size dependence of the bandgap[7] and the shift of the valence band.

In Fig. 4, the relative nanocrystal bandgap shifts with lowering temperature correspond to the shifts predicted by the 14-band k.p model, as illustrated in Fig. S2. The energies of the valence band maxima are within the accuracy of the measurement, all the same. This observation fits with the picture of the valence band being based on a quasi-flat (i.e., heavy mass) band as shown in Fig. 1(a). This makes the hole confinement energy weak and poorly dependent on particle size. Conversely, the conduction band accounts for most of the size-induced shift, as expected from a light, strongly dispersive band.

Since the shift results in a decrease in binding energy and appears rigid, the valence band moves closer to the Fermi level, making the material more *p*-type (or less *n*-type). Because the shift is similar for all NC sizes (Fig. 3 and S5), the effect is more pronounced for narrower bandgaps. From the perspective of a photodiode, temperature reduction can induce a 100 meV shift [Fig. 4(b)] in the energy of one of the carriers within a 350 meV optical bandgap. Such a Schottky barrier becomes even more difficult to overcome at reduced operating temperatures. Assuming the Schottky barrier is overcome through an Arrhenius process, the efficiency drops resulting from the temperature-induced absolute energy shift (Φ_B), can be estimated as $\exp(-|\Phi_B|/k_BT) \approx 10^{-3}$, for operation at 173 K. This may require a substantial redesign of the photodiode and illustrates the specific challenges relative to mid-IR sensitive NCs. Charge transport layers developed for the visible and even near-infrared ranges are difficult to transfer, not only because of the presence of a massive offset but also because the design strategy must account for the actual targeted operating temperature. Absolute positioning of the band edges constitutes a level of refinement certainly necessary for the development of the next generation of MWIR NC-based photodetectors.

In conclusion, we have investigated *in situ*, using X-ray photoemission spectroscopy, the absolute energy shift of the electronic spectrum of HgTe NCs of various sizes relevant for infrared sensing. Upon cooling to temperatures typical of infrared sensor operation, we observe a rigid shift of the electronic spectrum, reaching about 100 meV at 80 K. This shift appears barely dependent on particle size or band edge energy. Consequently, the resulting corrections in carrier density and the formation of Schottky interface barriers are more severe for narrow-bandgap materials, which are particularly important for mid-infrared sensing.

See the supplementary material for details on (i) the method for sample growth and preparation, (ii) the 14-band k.p modeling of HgTe, (iii) the activation energy of the dark current, and (iv) additional data documenting the thermal shift of the photoemission spectra.

The project was supported by the ERC grant AQDtive (Grant No. 101086358) and from the French National Research Agency (ANR) through the grants MixDferro (ANR-21-CE09-0029), Quicktera (ANR-22-CE09-0018), Operatwist (ANR-22-CE09-0037-01), E-map (ANR-23-CE50-0025), DIRAC (ANR-24-ASM1-0001), camIR (ANR-24-CE42-2757), and Piquant (ANR-24-CE09-0786). We acknowledge the use of clean-room facilities from the "Centrale de Proximité Paris-Centre" and support from Renatech+ for micro and nanofabrication. This project has also received financial support from the CNRS through the MITI interdisciplinary programs (project WITHIN) and Region Ile de France through Sesame project INSIDE.

AUTHOR DECLARATIONS

Conflict of Interest

The authors have no conflicts to disclose.

Author Contributions

Tommaso Gemo and Dario Mastrippolito contributed equally to this work.

Tommaso Gemo: Formal analysis (equal); Writing – original draft (equal); Writing – review & editing (equal). **Dario Mastrippolito:** Data curation (lead); Formal analysis (lead); Investigation (lead); Methodology (lead); Writing – original draft (lead); Writing – review & editing (lead). **Mariarosa Cavallo:** Formal analysis (equal); Investigation (equal); Methodology (equal); Validation (equal); Writing – original draft (equal); Writing – review & editing (equal). **Giorgia Strobbia:** Formal analysis (equal); Investigation (equal); Writing – review & editing (equal). **Albin Colle:** Investigation (equal); Writing – review & editing (equal). **Marco Paye:** Investigation (equal); Writing – review & editing (equal). **Jiho Roh:** Investigation (equal); Writing – review & editing (equal). **Adrien Khalili:** Investigation (equal); Writing – review & editing (equal). **Clement Gureghian:** Investigation (equal); Writing – review & editing (equal). **Erwan Bossavit:** Investigation (equal); Methodology (equal); Validation (equal); Writing – review & editing (equal). **Sandrine Ithurria:** Funding acquisition (equal); Project administration (equal); Writing – review & editing (equal). **Yoann Prado:** Formal analysis (equal); Investigation (equal); Writing – review & editing (equal). **Sébastien Sauvage:** Conceptualization (equal); Data curation (equal); Formal analysis (equal); Investigation (equal); Writing – original draft (equal); Writing – review & editing (equal). **Mathieu G. Silly:** Formal analysis (equal); Funding acquisition (equal); Methodology (equal); Resources (equal); Writing – review & editing (equal). **Nicolas Péré-Laperne:** Conceptualization (equal); Funding acquisition (equal); Project administration (equal); Supervision (equal); Writing – review & editing (equal). **Debora Pierucci:** Conceptualization (equal); Data curation (equal); Formal analysis (equal); Funding acquisition (equal); Investigation (equal); Validation (equal); Writing – original draft (equal); Writing – review & editing (equal). **Emmanuel Lhuillier:** Conceptualization (equal); Formal analysis (equal); Funding acquisition (equal); Resources (equal); Supervision (equal); Validation (equal); Writing – original draft (equal); Writing – review & editing (equal).

DATA AVAILABILITY

The data that support the findings of this study are available from the corresponding author upon request.

REFERENCES

[1]S. Richard, F. Aniel, and G. Fishman, "Energy-band structure of Ge, Si, and GaAs: A thirty-band k.p method," Phys. Rev. B **70**(23), 235204 (2004).

[2]M. El Kurdi, S. Sauvage, G. Fishman, and P. Boucaud, "Band-edge alignment of SiGe/Si quantum wells and SiGe/Si self-assembled islands," Phys. Rev. B **73**(19), 195327 (2006).

[3]N. A. Čukarić, M. Ž. Tadić, B. Partoens, and F. M. Peeters, "30-band k.p model of electron and hole states in silicon quantum wells," Phys. Rev. B **88**(20), 205306 (2013).

[4]R. Dornhaus, G. Nimtz, and B. Schlicht, "Narrow-gap semiconductors," in *Springer Tracts in Modern Physics* (Springer, 1983).

[5]K. A. Sergeeva, H. Zhang, A. S. Portniagin, E. Bossavit, G. Mu, S. V. Kershaw, S. Ithurria, P. Guyot-Sionnest, S. Keuleyan, C. Delerue, X. Tang, A. L. Rogach, and E. Lhuillier, "The rise of HgTe colloidal quantum dots for infrared optoelectronics," Adv. Funct. Mater. **34**(39), 2405307 (2024).

[6]C. Gréboval, A. Chu, N. Goubet, C. Livache, S. Ithurria, and E. Lhuillier, "Mercury chalcogenide quantum dots: Material perspective for device integration," Chem. Rev. **121**(7), 3627–3700 (2021).

[7]N. Moghaddam, C. Gréboval, J. Qu, A. Chu, P. Rastogi, C. Livache, A. Khalili, X. Z. Xu, B. Baptiste, S. Klotz, G. Fishman, F. Capitani, S. Ithurria, S. Sauvage, and E. Lhuillier, "The strong confinement regime in HgTe two-dimensional nanoplatelets," J. Phys. Chem. C **124**(42), 23460–23468 (2020).

[8]J. Black, S. M. Ku, and H. T. Minden, "Some semiconducting properties of HgTe," J. Electrochem. Soc. **105**(12), 723 (1958).

[9]T. C. Harman, M. J. Logan, and H. L. Goering, "Preparation and electrical properties of mercury telluride," J. Phys. Chem. Solids **7**(2), 228–235 (1958).

[10]J. Baars and F. Sorger, "Reststrahlen spectra of HgTe and $Cd_xHg_{1-x}Te$," Solid State Commun. **10**(9), 875–878 (1972).

[11]Y. Tian, H. Luo, M. Chen, C. V. Li, S. Kershaw, R. L. Zhang, and A. Rogach, "Mercury chalcogenide colloidal quantum dots for infrared photodetection: From synthesis to device applications," Nanoscale **15**(14), 6476–6504 (2023).

[12]S. Keuleyan, E. Lhuillier, and P. Guyot-Sionnest, "Synthesis of colloidal HgTe quantum dots for narrow mid-IR emission and detection," J. Am. Chem. Soc. **133**(41), 16422–16424 (2011).

[13]A. Caillas and P. Guyot-Sionnest, "Uncooled high detectivity mid-infrared photoconductor using HgTe quantum dots and nanoantennas," ACS Nano **18**(12), 8952–8960 (2024).

[14]J. C. Peterson and P. Guyot-Sionnest, "Room-temperature 15% efficient mid-infrared HgTe colloidal quantum dot photodiodes," ACS Appl. Mater. Interfaces **15**(15), 19163–19169 (2023).

[15]G. Mu, X. Zheng, Y. Tan, Y. Liu, Q. Hao, K. Weng, and X. Tang, "Colloidal quantum-dot heterojunction imagers for room-temperature thermal imaging," Adv. Mater. **37**(10), e2416877 (2025).

[16]A. Rose, *Concepts in Photoconductivity and Allied Problems* (Interscience Publishers, 1963).

[17]E. Lhuillier, S. Keuleyan, P. Rekemeyer, and P. Guyot-Sionnest, "Thermal properties of mid-infrared colloidal quantum dot detectors," J. Appl. Phys. **110**(3), 033110 (2011).

[18]C. S. Guenzer and A. Bienenstock, "Temperature dependence of the HgTe band gap," Phys. Rev. B **8**(10), 4655–4667 (1973).

[19]M. Dobrowolska, A. Mycielski, and W. Dobrowolski, "Determination of temperature dependence of energy gap in HgTe by oscillatory magnetotransmission measurements," Solid State Commun. **27**(11), 1233–1235 (1978).

[20]E. Lhuillier, S. Keuleyan, and P. Guyot-Sionnest, "Optical properties of HgTe colloidal quantum dots," Nanotechnology **23**(17), 175705 (2012).

[21]A. Olkhovets, R.-C. Hsu, A. Lipovskii, and F. W. Wise, "Size-dependent temperature variation of the energy gap in lead-salt quantum dots," Phys. Rev. Lett. **81**(16), 3539–3542 (1998).

[22]P. Man and D. S. Pan, "Infrared absorption in HgTe," Phys. Rev. B **44**(16), 8745–8758 (1991).

[23]H. Hu, J. Liu, J. Liu, M. Yuan, H. Ma, B. Wang, Y. Wang, H. Xia, J. Yang, L. Gao, J. Zhang, J. Tang, and X. Lan, "Double-heterojunction-based HgTe colloidal quantum dot imagers," ACS Nano **19**(9), 8974–8984 (2025).

[24]C. Gréboval, E. Izquierdo, C. Abadie, A. Khalili, M. Cavallo, A. Chu, T. H. Dang, H. Zhang, X. Lafosse, M. Rosticher, X. Z. Xu, A. Descamps-Mandine, A. Ouerghi, M. G. Silly, S. Ithurria, and E. Lhuillier, "HgTe nanocrystal-based photodiode for extended short-wave infrared sensing with optimized electron extraction and injection," ACS Appl. Nano Mater. **5**(6), 8602–8611 (2022).

[25]P. Rastogi, E. Izquierdo, C. Gréboval, M. Cavallo, A. Chu, T. H. Dang, A. Khalili, C. Abadie, R. Alchaar, S. Pierini, H. Cruguel, N. Witkowski, J. K. Utterback, T. Brule, X. Z. Xu, P. Hollander, A. Ouerghi, B. Gallas, M. G. Silly, and E. Lhuillier, "Extended short-wave photodiode based on CdSe/HgTe/Ag_2Te stack with high internal efficiency," J. Phys. Chem. C **126**(32), 13720–13728 (2022).

[26]J. Yang, Y. Lv, Z. He, B. Wang, S. Chen, F. Xiao, H. Hu, M. Yu, H. Liu, X. Lan, H.-Y. Hsu, H. Song, and J. Tang, "Bi_2S_3 electron transport layer incorporation for high-performance heterostructure HgTe colloidal quantum dot infrared photodetectors," ACS Photonics **10**(7), 2226–2233 (2023).

[27]X. Xue, M. Chen, Y. Luo, T. Qin, X. Tang, and Q. Hao, "High-operating-temperature mid-infrared photodetectors via quantum dot gradient homojunction," Light **12**(1), 2 (2023).
[28]M. M. Ackerman, X. Tang, and P. Guyot-Sionnest, "Fast and sensitive colloidal quantum dot mid-wave infrared photodetectors," ACS Nano **12**(7), 7264–7271 (2018).
[29]H. Zhang, R. Alchaar, Y. Prado, A. Khalili, C. Gréboval, M. Cavallo, E. Bossavit, C. Dabard, T. H. Dang, C. Abadie, C. Methivier, D. Darson, V. Parahyba, P. Potet, J. Ramade, M. G. Silly, J. K. Utterback, D. Pierucci, S. Ithurria, and E. Lhuillier, "Material perspective on HgTe nanocrystal-based short-wave infrared focal plane arrays," Chem. Mater. **34**(24), 10964–10972 (2022).